Journal of Zhejiang University-SCIENCE C (Computers & Electronics)
ISSN 1869-1951 (Print); ISSN 1869-196X (Online)
www.zju.edu.cn/jzus; www.springerlink.com
E-mail: jzus@zju.edu.cn

A sparse matrix model-based optical proximity correction algorithm with model-based mapping between segments and control sites

Bin LIN†, Xiao-lang YAN, Zheng SHI, Yi-wei YANG
(*Institute of VLSI Design, Zhejiang University, Hangzhou 310027, China*)
†E-mail: linbin@vlsi.zju.edu.cn

Received June 24, 2010; Revision accepted Sept. 26, 2010; Crosschecked Mar. 31, 2011

Abstract: Optical proximity correction (OPC) is a key step in modern integrated circuit (IC) manufacturing. The quality of model-based OPC (MB-OPC) is directly determined by segment offsets after OPC processing. However, in conventional MB-OPC, the intensity of a control site is adjusted only by the movement of its corresponding segment; this scheme is no longer accurate enough as the lithography process advances. On the other hand, matrix MB-OPC is too time-consuming to become practical. In this paper, we propose a new sparse matrix MB-OPC algorithm with model-based mapping between segments and control sites. We put forward the concept of 'sensitive area'. When the Jacobian matrix used in the matrix MB-OPC is evaluated, only the elements that correspond to the segments in the sensitive area of every control site need to be calculated, while the others can be set to 0. The new algorithm can effectively improve the sparsity of the Jacobian matrix, and hence reduce the computations. Both theoretical analysis and experiments show that the sparse matrix MB-OPC with model-based mapping is more accurate than conventional MB-OPC, and much faster than matrix MB-OPC while maintaining high accuracy.

Key words: Matrix sparsity, Optical proximity correction (OPC), Convergence, Segment, Sensitive area
doi:10.1631/jzus.C1000219 **Document code:** A **CLC number:** TN47

1 Introduction

Optical lithography (Schellenberg, 2004) using a reduction projection exposure system has been widely used to produce very large scale integrated (VLSI) circuits. According to Moore's Law, integrated circuit (IC) density increases with the minimum feature size decreasing and approaching the resolution limit of optics. The resolution of optical lithography has been improved mainly by using large numerical aperture optics and short wavelength light sources. The numerical aperture is limited to 1, in principle, except for immersion lenses, and shortening of the wavelength of exposure light is restricted by light source, lens materials, and resist transparency. Advanced IC's feature size (e.g., 90 nm, 65 nm, 45 nm) is much smaller than the wavelength of exposure light (193 nm). In this sub-wavelength region, optical proximity effect (OPE) appears strongly and degrades the quality of the projected image. Consequently, optical proximity correction (OPC) is one of the most widely used resolution enhancement techniques (RETs) predistorting mask patterns such that the printed patterns will be as close to the desired shapes as possible. This is very important to keep the imaging fidelity in IC manufacturing (Yu *et al.*, 2007). Some examples of OPE and OPC are shown in Fig. 1 (Terasawa, 2000).

OPC algorithms can be classified as inverse lithography technology (ILT) and model-based OPC (MB-OPC) (Yu and Pan, 2007a). Conventional MB-OPC is workable for early 90–180 nm technology nodes. As the feature size continuously shrinks, the k1 process factor (Weeks, 2001), which is the

measure of lithography aggressiveness, decreases, while the layout becomes more complicated. Conventional MB-OPC cannot work very well under these circumstances. The main problem is on OPC convergence (Painter *et al*., 2004; Choi *et al*., 2006; Herold *et al*., 2006). For example, in Fig. 2, the segments on a line end are not convergent to suitable positions. Fig. 3 shows another example wherein a segment's position oscillates between two successive iterations and converges to the final position very slowly.

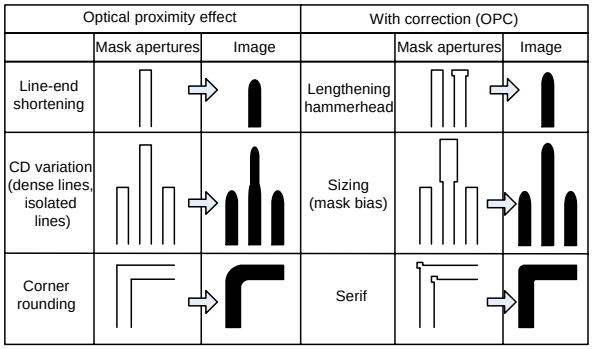

Fig. 1 Optical proximity effects and their correction (OPC) by modifying the mask apertures

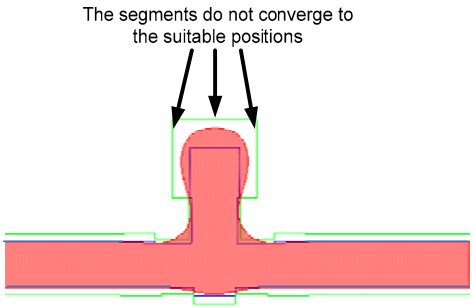

Fig. 2 Edge segments that do not converge after optical proximity correction

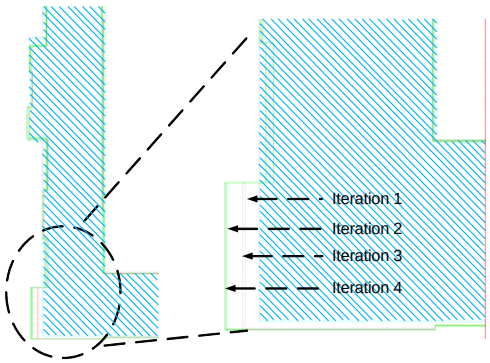

Fig. 3 A segment's position that oscillates and converges very slowly

To solve the convergence problem, Cobb and Granik (2002) proposed the matrix MB-OPC using the mask error enhancement factor (MEEF) matrix (Schellenberg *et al*., 1999; van Schoot *et al*., 1999; Granik, 2005). In matrix MB-OPC, not just one segment, but all the segments that influence the edge placement error (EPE), which stands for the difference between the printed contour and the target contour (Yu and Pan, 2007b), are used to control the EPE for a given site. Chen *et al*. (2007) used the Jacobian matrix of intensity distribution functions instead of the MEEF matrix in matrix MB-OPC to improve the algorithm.

Although the convergence problem can be partly solved by matrix MB-OPC, it takes a longer time to achieve a result, as Fig. 4 shows. The evaluation of the Jacobian matrix is the most time-consuming part, accounting for more than 50% of the total running time.

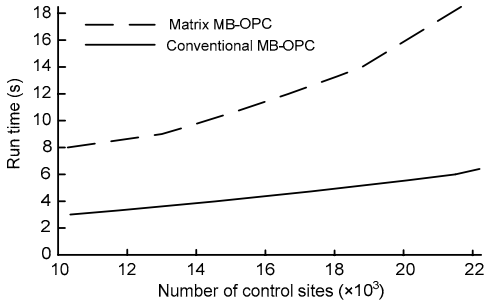

Fig. 4 Run time comparison between matrix model-based optical proximity correction (MB-OPC) and conventional MB-OPC for an exemplary layout

To improve the quality of MB-OPC with an acceptable running time, we propose a new sparse matrix MB-OPC algorithm with model-based mapping between segments and control sites.

2 Preliminaries

The lithography model can be described as a sum of coherent systems (SOCS) (Cobb *et al*., 1996) based on Hopkins' imaging equation (Hopkins, 1953). The intensity of point (x, y) with the mask environment M can be calculated by (Cobb and Zakhor, 1995)

$$I(x,y;M)=\sum_{i=1}^{n}\lambda_i\,|\,\Phi_i\otimes M\,|^2\,, \qquad (1)$$

where λ_i is the ith weight value, Φ_i is the ith

convolution kernel, n is the number of kernels, M is the polygon on mask in the kernel ambit area with point (x, y) as the center, and '⊗' is the convolution operator. Fig. 5 shows a group of convolution kernels. Fig. 6 shows an example of the ambit window.

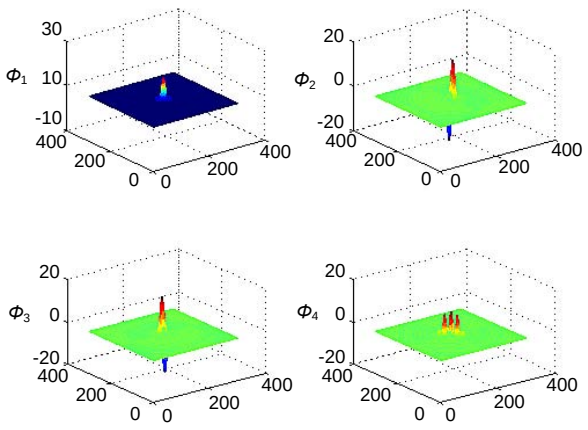

Fig. 5 Typical convolution kernel shapes

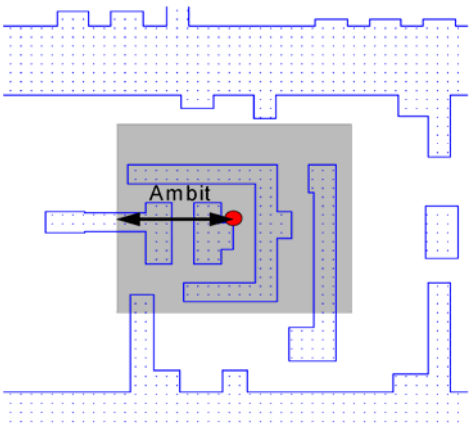

Fig. 6 An example of the ambit window

MB-OPC can be roughly divided into two steps, namely the dissection step and the correction step (Word *et al*., 2005; Chen *et al*., 2007). In the dissection step, the polygon edges in layout are dissected into small segments with a control site on each segment. In the correction step, the intensity profile and EPE are calculated at the control site for every segment, and then the segments are moved along their normal directions to make the intensity of the corresponding control site close to threshold (Weeks, 2001) and minimize the EPE. The accuracy of the MB-OPC result depends on both steps.

The aim of MB-OPC is to make the intensity of every control site close to the threshold through moving segments, and it can be described by

$$I(x_i, y_i; s_1, s_2, ..., s_n) = T_i, \quad i = 1, 2, ..., n, \tag{2}$$

where (x_i, y_i) are the coordinates of the ith control site, s_i is the offset of the ith segment, and T_i is the ith threshold of the control site. All the T_i's have the same value for the constant threshold resist (CTR) model and they have different values for the variable threshold resist (VTR) model where they are a function of aerial image properties, such as intensity and slope.

In conventional MB-OPC, to make the intensity of a control site close to the threshold, only one segment with a control site on it is moved. Hence, Eq. (2) is simply approximated to

$$I(x_i, y_i; s_i) = T_i, \quad i = 1, 2, ..., n. \tag{3}$$

In the matrix MB-OPC algorithm proposed by Chen *et al*. (2007), Newton's method is used to obtain the least square solution of Eq. (2), as shown in the following steps:

1. Solving the system of linear equations

$$J(\boldsymbol{s}_k)\boldsymbol{d}_k = -[I(\boldsymbol{s}_k) - T(\boldsymbol{s}_k)], \tag{4}$$

where $\boldsymbol{s}_k$, $\boldsymbol{d}_k \in \mathbb{R}^n$, $\boldsymbol{s}_k$ is the vector of the total offset of each segment at loop k, $J(\boldsymbol{s}_k)$ means the Jacobian matrix at s_k, $I(\boldsymbol{s}_k)$ and $T(\boldsymbol{s}_k)$ are the vectors of intensity and threshold of each control site at loop k, respectively, and $\boldsymbol{d}_k$ means the vector of the offset of each segment at loop k.

2. Updating offsets

$$\boldsymbol{s}_{k+1} = \boldsymbol{s}_k + \boldsymbol{d}_k. \tag{5}$$

The Jacobian matrix of Eq. (4) is defined as

$$\boldsymbol{J} = \begin{bmatrix} \frac{\partial I_1}{\partial s_1} & \frac{\partial I_1}{\partial s_2} & \cdots & \frac{\partial I_1}{\partial s_n} \\ \frac{\partial I_2}{\partial s_1} & \frac{\partial I_2}{\partial s_2} & \cdots & \frac{\partial I_2}{\partial s_n} \\ \vdots & \vdots & & \vdots \\ \frac{\partial I_n}{\partial s_1} & \frac{\partial I_n}{\partial s_2} & \cdots & \frac{\partial I_n}{\partial s_n} \end{bmatrix}, \tag{6}$$

when a CTR model is used.

3 Sparse matrix model-based OPC algorithm with model-based mapping

Suppose the mask environment $\boldsymbol{M}$ is represented by a matrix with each element denoted as M_{pq}. The derivative of intensity corresponding to each M_{pq} is obtained from Eq. (1):

$$\begin{aligned}
G_{pq} &= \frac{\partial I(x,y;\boldsymbol{M})}{\partial M_{pq}} \\
&= \frac{\partial}{\partial M_{pq}} \sum_{i=1}^{n} \lambda_i \left[(\mathrm{real}(\Phi_i) \otimes \boldsymbol{M})^2 + (\mathrm{imag}(\Phi_i) \otimes \boldsymbol{M})^2 \right] \\
&= \sum_{i=1}^{n} \lambda_i \left[\frac{\partial (\mathrm{real}(\Phi_i) \otimes \boldsymbol{M})^2}{\partial M_{pq}} \right] + \sum_{i=1}^{n} \lambda_i \left[\frac{\partial (\mathrm{imag}(\Phi_i) \otimes \boldsymbol{M})^2}{\partial M_{pq}} \right] \\
&= 2 \sum_{i=1}^{n} \lambda_i \left[(\mathrm{real}(\Phi_i) \otimes \boldsymbol{M}) \times \frac{\partial (\mathrm{real}(\Phi_i) \otimes \boldsymbol{M})}{\partial M_{pq}} \right] \\
&\quad + 2 \sum_{i=1}^{n} \lambda_i \left[(\mathrm{imag}(\Phi_i) \otimes \boldsymbol{M}) \times \frac{\partial (\mathrm{imag}(\Phi_i) \otimes \boldsymbol{M})}{\partial M_{pq}} \right] \\
&= 2 \sum_{i=1}^{n} \lambda_i \left[(\mathrm{real}(\Phi_i) \otimes \boldsymbol{M}) \times \mathrm{rot180}(\mathrm{real}(\Phi_i))_{pq} \right] \\
&\quad + 2 \sum_{i=1}^{n} \lambda_i \left[(\mathrm{imag}(\Phi_i) \otimes \boldsymbol{M}) \times \mathrm{rot180}(\mathrm{imag}(\Phi_i))_{pq} \right].
\end{aligned} \tag{7}$$

Thus, the matrix form of all derivatives is a gradient:

$$\begin{aligned}
\boldsymbol{G} &= \frac{\partial I(x,y;\boldsymbol{M})}{\partial \boldsymbol{M}} \\
&= \sum_{i=1}^{n} \left[C_{i,\mathrm{real}} \odot \mathrm{rot180}(\mathrm{real}(\Phi_i)) \right. \\
&\quad \left. + C_{i,\mathrm{imag}} \odot \mathrm{rot180}(\mathrm{imag}(\Phi_i)) \right],
\end{aligned} \tag{8}$$

where $C_{i,\mathrm{real}}=2\lambda_i(\mathrm{real}(\Phi_i)\otimes\boldsymbol{M})$, $C_{i,\mathrm{imag}}=2\lambda_i(\mathrm{imag}(\Phi_i)\otimes\boldsymbol{M})$, and '$\odot$' means two matrices multiply element by element.

The magnitude of the absolute values of elements of matrix $\boldsymbol{G}$ indicates the influence of mask change on the intensity change. Element M_{pq} with a large absolute value of gradient in matrix $\boldsymbol{G}$ contributes more to the intensity than other elements.

Matrix $\boldsymbol{G}$ is considered as a weighted sum of the real and imaginary parts of kernels. For SOCS of a typical lithographic system, the first several kernels account for more than 90% of intensity; thus, not all kernels are needed to calculate $\boldsymbol{G}$. Table 1 shows an example of the kernel weights. In practice, only the first a few kernels are used. Also, the real and imaginary parts of a kernel sometimes differ in several orders of magnitude, which means the small part can be neglected.

Table 1 Kernel number and precision: an example*

Eigenvalue	Kernel number used	Similarity to Hopkins' equation (%)
116.207	1	89.8450
25.7721	2	97.8144
25.7721	3	98.6832
…	…	…
1.49803	12	99.9410

* λ=193 nm, NA=0.76, σ=0.73, defocus=120 nm

Sensitive area is an area in which the corresponding elements of $\boldsymbol{G}$ have larger absolute values than the others. That is, the moving of segments in the sensitive area has a more significant effect on the intensity than that of the others. Define $\boldsymbol{M}_{\mathrm{SA}}$ to be a matrix of the same size as kernels, in which the elements of value 1 together represent the sensitive area. The binary search method can be used to find $\boldsymbol{M}_{\mathrm{SA}}$, which makes Eq. (9) valid:

$$\sum_{i=1}^{n} \lambda_i \left| \Phi_i \otimes \boldsymbol{M}_{\mathrm{SA}} \right|^2 = a, \tag{9}$$

where a is a coefficient to adjust the sensitive area, and $0 \le a \le 1$.

The procedure is shown in Fig. 7, and an example of the result is shown in Fig. 8.

Different control sites have their respective sensitive areas. However, for different correction loops, it is not necessary to recompute the sensitive area because its variation caused by the variation of the mask is so slight. The offset of any segment in the sensitive area contributes more than the others out of the sensitive area to the intensity. Hence, the sensitive area determines the mapping between segments and control sites.

Figs. 9 and 10 are sensitive areas of lithography models with conventional illumination and annular illumination, respectively. Even when a=0.9, the sensitive area is still far smaller than the ambit window. This phenomenon means that, the intensity of every control site is determined mainly by the patterns in its corresponding small sensitive area. The offsets

of segments in the sensitive area play the major role in changing the intensity of the control site (Fig. 11). Therefore, when evaluating the Jacobian matrix described by Eq. (6), only the elements that correspond to the segments in the sensitive areas of the control sites need to be calculated. Thus, the time spent on the evaluation of the Jacobian matrix will be greatly reduced, and the correction accuracy will not be impacted much because of the reservation of main intensity contributors. Take the case of Fig. 10 as an example. When n=100 in Eq. (6), about 90% of the elements of the Jacobian matrix can be set to 0, and only 10% elements need to be calculated.

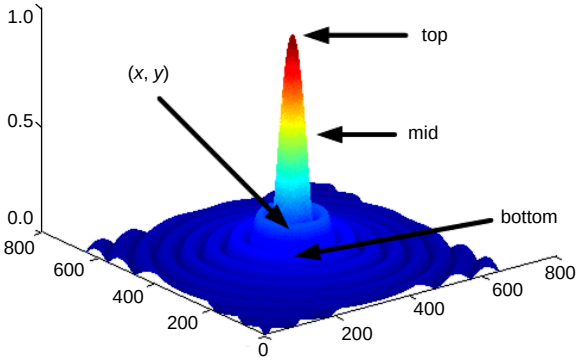

Step 1: top=max(|**G**|);
Step 2: bottom=min(|**G**|);
Step 3: mid=(top+bottom)/2;
Step 4: $\boldsymbol{M}_{SA}$=(|**G**|>mid);
Step 5: while $I(x, y; \boldsymbol{M}_{SA})$!=$a$
  if $I(x, y; \boldsymbol{M}_{SA})$>$a$
    bottom=mid;
  else
    top=mid;
  end if
  mid=(top+bottom)/2;
  $\boldsymbol{M}_{SA}$=(|**G**|>mid);
end while

Fig. 7 Schematic of the binary search method for $\boldsymbol{M}_{SA}$

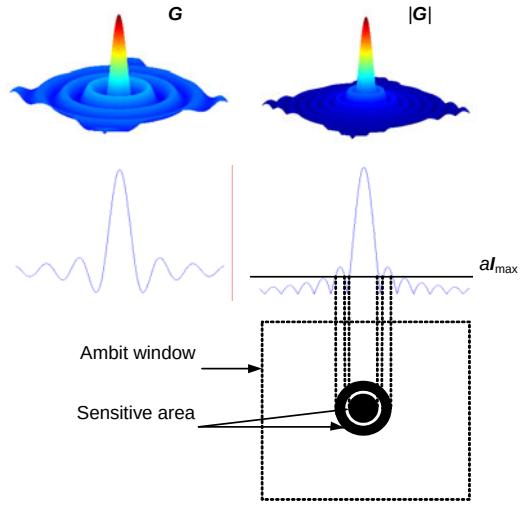

Fig. 8 An example of the sensitive area derived from matrix $\boldsymbol{G}$

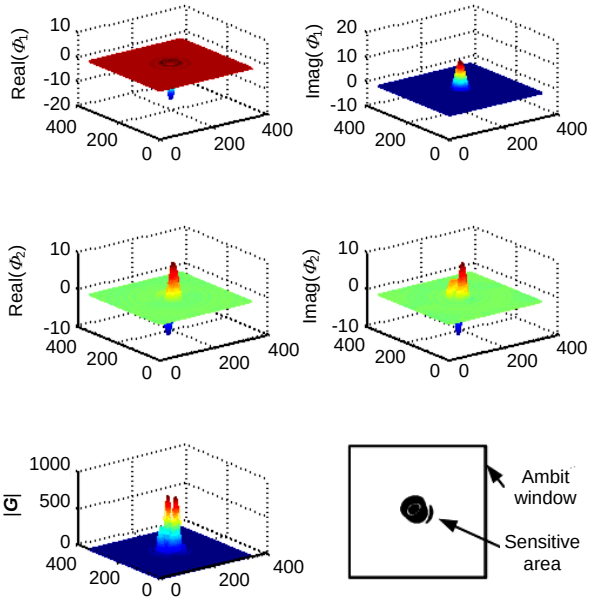

Fig. 9 The first two kernels of the conventional illumination lithography model and the corresponding absolute gradient |G| and sensitive area
λ=193 nm, NA=0.76, σ=0.73, defocus=120 nm, a=0.9

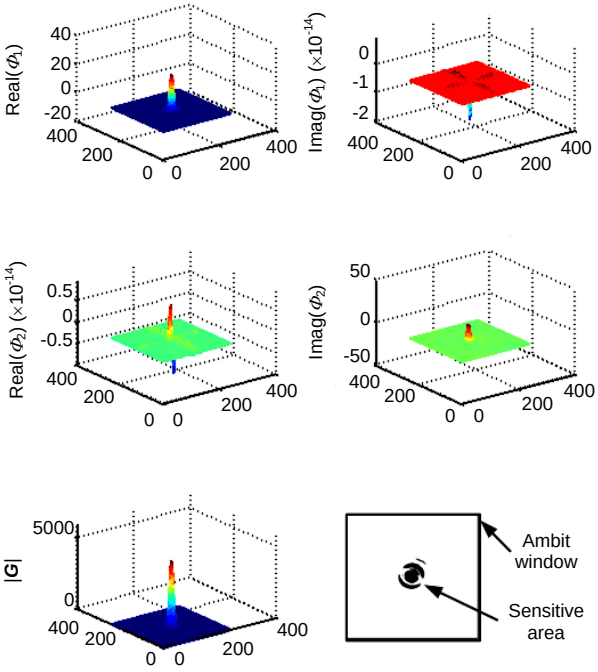

Fig. 10 The first two kernels of the annular illumination lithography model and the corresponding absolute gradient |G| and sensitive area
λ=193 nm, NA=0.78, σ=0.85, inner σ'=0.5, a=0.9

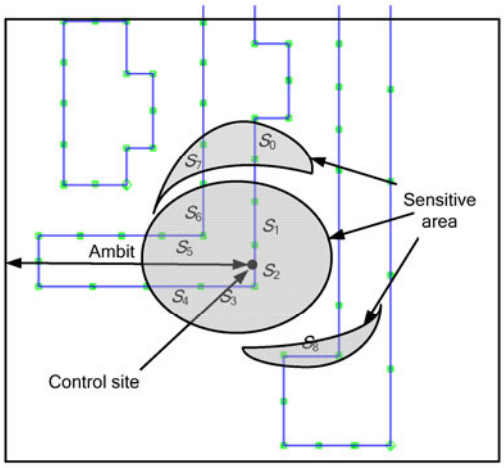

Fig. 11 Segments in the sensitive area playing a major role in changing the intensity of the control site
Only the elements that correspond to the segments in the sensitive areas need to be calculated when evaluating the Jacobian matrix

The mapping between segments and control sites is determined by the sensitive area. In this sparse matrix MB-OPC, all the operations are the same as in the matrix MB-OPC introduced in Chen *et al*. (2007), except the insertion of the sensitive area generation step and the mapping step (Fig. 12). The mapping step maps between segments and control sites based on the sensitive area to cut down the time spent on Jacobian matrix evaluation.

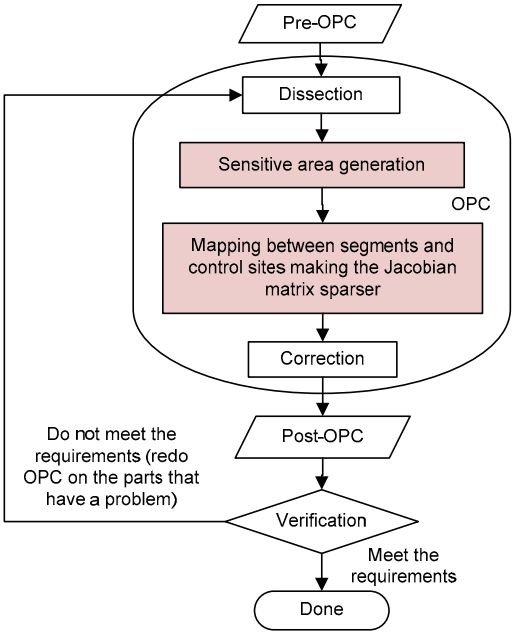

Fig. 12 The flowchart of sparse matrix model-based optical proximity correction (OPC) and verification

4 Experiments and comparison

Three 90 nm layouts with an area of 3 mm×3 mm were used in the experiments and some examples are shown here. The parameters of the lithography model were λ=193 nm, NA=0.76, and annular illumination with σ=0.56–0.80. 'Ambit' of the process model was set to 1000 nm. All computations were performed on a Dell PowerEdge 2950 workstation (Xeon 2.5 GHz×8 CPUs and 16 GB memory).

Fig. 13 shows the comparison of run time of conventional MB-OPC, matrix MB-OPC, and the proposed sparse matrix MB-OPC. Run time spent on sparse matrix MB-OPC with a mapping step between segments and control sites is much less than that on the matrix MB-OPC.

Fig. 14 compares the residual EPE of the three kinds of MB-OPC. The EPE distributions of matrix MB-OPC and sparse matrix MB-OPC with a mapping step between segments and control sites, both of which concentrate around 0 nm, are similar and much better than that of the conventional MB-OPC.

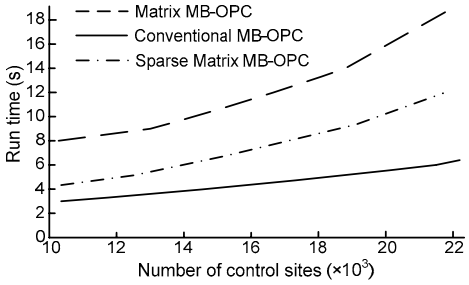

Fig. 13 Run time of conventional model-based optical proximity correction (MB-OPC), matrix MB-OPC, and sparse matrix MB-OPC

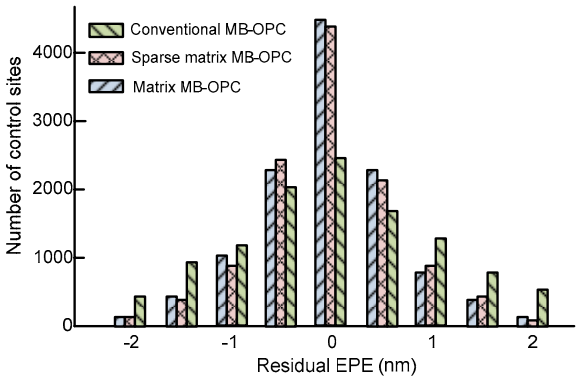

Fig. 14 Residual edge placement error (EPE) distributions of sparse matrix model-based optical proximity correction (MB-OPC), matrix MB-OPC, and conventional MB-OPC

Fig. 15 shows a piece of layout corrected by our sparse matrix MB-OPC, in which the simulated contours of post-OPC are much closer to the original layout than the contours of pre-OPC.

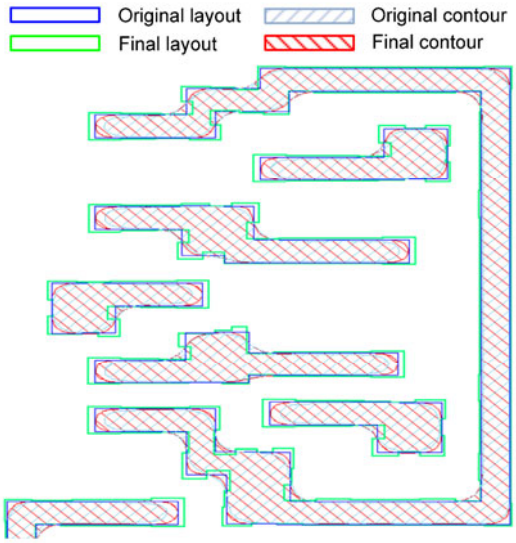

Fig. 15 An example of using sparse matrix model-based optical proximity correction (MB-OPC)

5 Conclusions

This paper presents a new kind of sparse matrix MB-OPC algorithm with model-based mapping between segments and control sites. The key innovative part of this method is the mapping step between segments and control sites based on a sensitive area, which greatly reduces the computations of the OPC process. Experiments show that the sparse matrix MB-OPC algorithm with model-based mapping between segments and control sites has almost the same accuracy performance as matrix MB-OPC and significantly improves the OPC speed.

References

Chen, Y., Wu, K., Shi, Z., Yan, X.L., 2007. A feasible model-based OPC algorithm using Jacobian matrix of intensity distribution functions. *SPIE*, **6520**:65204C1-65204C10. [doi:10.1117/12.711763]

Choi, S.H., Je, A.Y., Hong, J.S., Yoo, M.H., Kong, J.T., 2006. Meef-based correction to achieve OPC convergence of low-k1 lithography with strong OAI. *SPIE*, **6154**: 61540P-1-61540P-9. [doi:10.1117/12.656894]

Cobb, N.B., Granik, Y., 2002. Model-based OPC using the meef matrix. *SPIE*, **4889**:1281-1292. [doi:10.1117/12.467435]

Cobb, N.B., Zakhor, A., 1995. Fast sparse aerial image calculation for OPC. *SPIE*, **2621**:534-545. [doi:10.1117/12.228208]

Cobb, N.B., Zakhor, A., Miloslavsky, E., 1996. Mathematical and CAD framework for proximity correction. *SPIE*, **2726**:208-222. [doi:10.1117/12.240907]

Granik, Y., 2005. Generalized mask error enhancement factor theory. *J. Microlithogr. Microfabr. Microsyst.*, **4**(2): 023001-1-023001-10. [doi:10.1117/1.1898066]

Herold, K., Chen, N., Stobert, I.P., 2006. Managing high-accuracy and fast convergence in OPC. *SPIE*, **6349**:634924-1-634924-8. [doi:10.1117/12.686725]

Hopkins, H.H., 1953. On the diffraction theory of optical images. *Proc. R. Soc. A*, **217**(1130):408-432. [doi:10.1098/rspa.1953.0071]

Painter, B., Melvin, L.S.III, Rieger, M.L., 2004. Classical control theory applied to OPC correction segment convergence. *SPIE*, **5377**:1198-1206. [doi:10.1117/12.537586]

Schellenberg, F.M., 2004. Resolution enhancement technology: the past, the present, and extensions for the future. *SPIE*, **5377**:1-20. [doi:10.1117/12.548923]

Schellenberg, F.M., Boksha, V., Cobb, N., Lai, J.C., Chen, C.H., Mack, C., 1999. Impact of mask errors on full chip error budgets. *SPIE*, **3679**:261-272. [doi:10.1117/12.354339]

Terasawa, T., 2000. Subwavelength optical lithography. *SPIE*, **4181**:8-16. [doi:10.1117/12.395721]

van Schoot, J., Finders, J., Schenau, K.V.I., Klaassen, M., Buijk, C., 1999. Mask error factor: causes and implications for process latitude. *SPIE*, **3679**:250-260. [doi:10.1117/12.354338]

Weeks, R.Jr., 2001. Resolution Enhancement Techniques. SPIE Press, Bellingham, Washington, USA, p.18-30.

Word, J., Torres, A., Lacour, P., 2005. Advanced layout fragmentation and simulation schemes for model based OPC. *SPIE*, **5754**:1159-1168. [doi:10.1117/12.598848]

Yu, P., Pan, D.Z., 2007a. TIP-OPC: a New Topological Invariant Paradigm for Pixel Based Optical Proximity Correction. Proc. IEEE/ACM Int. Conf. on Computer-Aided Design, p.847-853. [doi:10.1109/ICCAD.2007.4397370]

Yu, P., Pan, D.Z., 2007b. A Novel Intensity Based OPC Algorithm with Speedup in Lithography Simulation. Proc. IEEE/ACM Int. Conf. on Computer-Aided Design, p.854-859. [doi:10.1109/ICCAD.2007.4397371]

Yu, P., Shi, S.X., Pan, D.Z., 2007. True process variation aware optical proximity correction with variational lithography modeling and model calibration. *J. Microlithogr. Microfabr. Microsyst.*, **6**(3):031004. [doi:10.1117/1.2752814]